Near-Eye Display for Vision Correction with Large FOV

Yishi Wu, Chao Ping Chen, Lei Zhou, Yang Li, Bing Yu, Huayi Jin*

Smart Display Lab, Department of Electronic Engineering, Shanghai Jiao Tong University, Shanghai, China
Email: ccp@sjtu.edu.cn

Abstract

We propose a see-through near-eye display capable of visual correction for -3.00-diopter myopia. Our solution features a freeform waveguide, which integrates a corrective lens and multiplexed volume holograms. Its key performance including diffraction efficiency, field of view, modulation transfer function, and distortion has been studied.

Keywords

near-eye display; vision correction; freeform waveguide; multiplexed volume holograms.

1. Introduction

See-through near-eye display (NED) is one of the key components of augmented reality (AR), as it serves as an interface connecting both real and virtual worlds. Generally, see-through NED can be categorized into three main families—combiner-based [1-3], waveguide-based [4-8], and retinal-projection-based [9,10]. Combiner-based NEDs usually adopt beam splitters [2] or semi-reflective mirrors [1], through which real and virtual images could overlay with each other. Due to the size of beam splitters and semi-reflective mirrors, such NEDs—if designed with a large field of view (FOV)—are often bulky and heavy. Waveguide-based NEDs can be designed with a compact form factor by using planar waveguides [5,6]. But once the light enters into a waveguide, the minimum angle, at which it could leave, will be confined by the total internal reflection. For this reason, FOVs of those NEDs largely hinge on the types of elements for out-coupling. Retinal-projection-based NEDs can project images directly onto the retina. However, there is an intrinsic problem associated with the retinal-projection-based NED in that the image formed on the retina is subject to the change of eye's focus [9].

Unlike flat panel displays, *e.g.* liquid crystal display (LCD) [11] and organic light-emitting diode (OLED) [12], NED is also a wearable device that is close to the eyes. Therefore, optics aside, ergonomics needs to be taken into account as well. One of the ergonomic issues is how to save the visually impaired users from the trouble of wearing extra eyeglasses or contact lens. As an earlier attempt, we introduced a combiner-based NED that enables the vision correction for myopia [13-15]. In this paper, we propose a compact design of see-through NED, highlighted by a freeform waveguide, which is essentially an integration of a corrective lens, a reflective surface, and multiplexed volume holograms (VHs). The proposed structure, design principle, and simulation results are to be elaborated in what follows.

2. Proposed Structure

The proposed structure of our NED solution is depicted in Fig. 1. It mainly consists of a 0.47" microdisplay, a 4-element projection lens, and a freeform waveguide. On the freeform waveguide are coated a curved, reflective surface, acting as an in-coupler, and multiplexed VHs, acting as an out-coupler. The projection lens is composed of four different lenses to project the magnified virtual image and to collimate the light into a small entrance pupil. After entering the waveguide, the collimated light will first be reflected by the reflective surface, undergo a total internal reflection, and then be coupled out by the multiplexed VHs. In our design, the lower surface of the waveguide assumes a concave surface, which would exactly match with the focus of the visually impaired eyes. As for the aberration, the lower surface is designed to be aspherical.

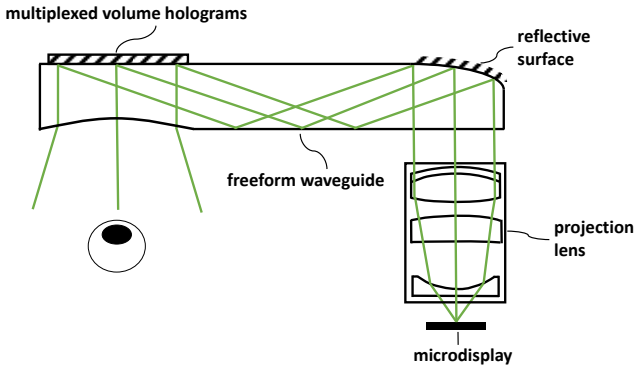

Figure 1. Schematic drawing of the proposed NED.

3. Design Principle

The FOV of the near-eye display depends on the FOV of the projection lens and the angular bandwidth of the multiplexed VHs. The FOV of the projection lens is 54°, which can be derived as

$$FOV = 2\arctan\left(\frac{D}{2f_p}\right) \tag{1}$$

where D is the diagonal dimension of the microdisplay, which is 0.47" (11.938 mm) in our design. f_p is the effective focal length of the projection lens, which is 11.68 mm according to the simulation results.

The FOV of our near-eye display could be limited by the angular bandwidth of the multiplexed VHs. The period Λ of a single VH is given by

$$\Lambda = \frac{\lambda_c}{2\sin\left(\theta/2\right)} \tag{2}$$

where λ_c is the construction wavelength of the VH and θ is the angle between object light and reference light.

Recalling Bragg's condition [16], θ_B is Bragg angle, which can be derived as

$$\sin\theta_B = \frac{\lambda\sin\left(\theta/2\right)}{\lambda_c} \tag{3}$$

where λ is the incident wavelength. Since our design is monochromatic, we let $\lambda = \lambda_c$.

According to Kogelnik's coupled wave theory [17], a VH is highly selective on the incident angles. When the incident angle deviates from the Bragg angle, the diffraction efficiency (DE) drops dramatically. To obtain a larger angular bandwidth, different VHs are multiplexed into one layer through three times of exposure. Due to the existence of the side lobes, DE curves of the multiplexed VHs will be partially overlapped, the overall diffraction efficiency η can be calculated as [15]

$$\eta = \eta_1 + (1-\eta_1)\eta_2 + (1-\eta_1)(1-\eta_2)\eta_3 \qquad (4)$$

The software VirtualLab Fusion (Wyrowski Photonics), based on the Fourier modal method [18], is used to calculate the DE of VHs. The individual DE as well as the multiplexed one is calculated versus the incident angle, as shown in Fig. 2. The parameters used are listed in Table 1.

Table 1. Parameters of three-multiplexed VHs

	θ/°	θ_B/°	Λ/nm
VH1	28.0	14.0	1099.5
VH2	52.0	26.0	606.8
VH3	80.0	40.0	413.8
$\lambda_c = \lambda = 532$ nm, $d = 10$ μm, $n_{avg} = 1.51$, $\delta_n = 0.06$			

As shown in Fig. 2, the full width at half maximum (FWHM) of the multiplexed DE is 48° (0°-48°). If NED works within this angular range, it can be said that the FOV of multiplexed VHs is 48° horizontally. Given a microdisplay with an aspect ratio of 16:9, the corresponding diagonal FOV of multiplexed VHs is 54°, which well matches the diagonal FOV of the projection lens.

The diffraction uniformity Γ is defined as

$$\Gamma = 1 - \frac{\sigma}{\eta_{avg}} \qquad (5)$$

where η_{avg} is the average DE and σ is the standard deviation of a set of DEs sampled from Fig. 2. By sampling the region of FWHM at an interval of 1°, we could find out that η_{avg}=87%, σ=12%, and Γ=96%. For a better uniformity, VHs shall be more overlapped.

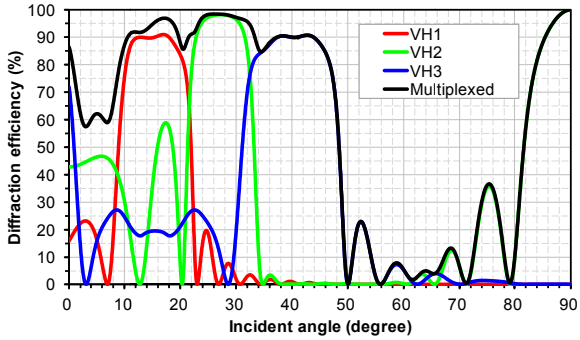

Figure 2. Calculated DE with respect to incident angles.

4. Results and Discussion

The software Code V (Synopsys), based on the ray tracing, is employed to analyze the imaging properties, including modulation transfer function (MTF), distortion, and imaging simulation. The design wavelength is 532 nm. Parameters for defining spherical and aspherical surfaces used in our simulation are summarized in Table 2 and Table 3, respectively. Fig. 3 shows a 3D view of the system, with all surfaces being labelled.

The diffraction MTFs at the central and marginal FOVs are plotted in Fig. 4, where MTFs of the real image are above 0.4 at 140 cycle/mm, and MTFs of the virtual image are above 0.4 at 13 cycles/mm.

Table 2. Surface parameters used in Code V

Surface	Surface Type	Sequential (Y/N)	Radius (mm)	Thickness (mm)	Refractive index[a]
Object	sphere	Y	infinity	9.2490	
1	sphere	Y	infinity	1.0396	1.58
2	sphere	Y	10.7020	7.4878	
3	asphere	Y	70.3754	0.9002	1.63
4	sphere	Y	-59.0083	1.8518	
5	asphere	Y	39.2785	1.2596	1.62
6	asphere	Y	-14.5984	2.0000	1.73
7	sphere	Y	-17.3685	14.1804	
stop	sphere	Y	infinity	5.6521	
9	XY poly	N	-4711.127	0.0000	1.20
10	sphere	N	infinity	0.0000	
11	sphere	N	infinity	0.0000	
12	asphere	Y	167.0000	249.5919	
image	sphere	Y	infinity	48.8535	

[a]Refractive index is left empty when the medium is air.

Table 3. Detailed parameters for aspherical surfaces

Surface	Conic constant (K)	4th order coefficient (A)	6th order coefficient (B)	8th order coefficient (C)
3	432.1221	0.0011	4.5903E-05	8.2510E-05
5	-0.0069	-5.2177E-08	2.0272E-07	9.1744E-09
6	0.8076	4.4325E-05	8.8053E-06	1.2005E-07
12	-2.9203	0.0002	-1.4257E-05	-1.6187E-06

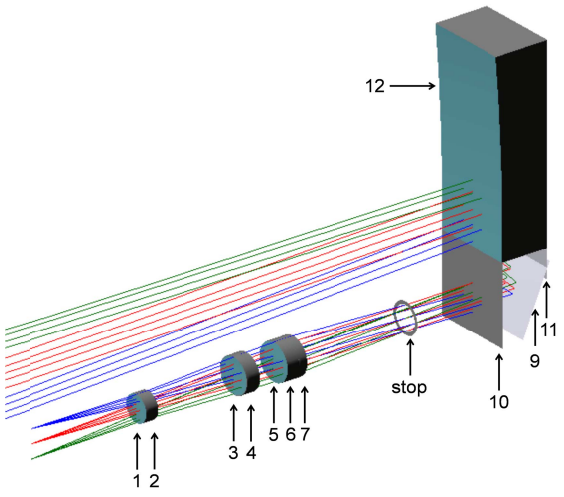

Figure 3. 3D view of our NED system.

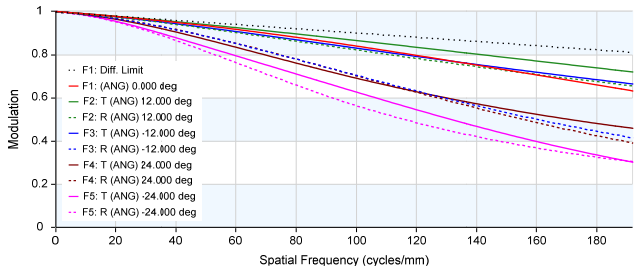

(a)

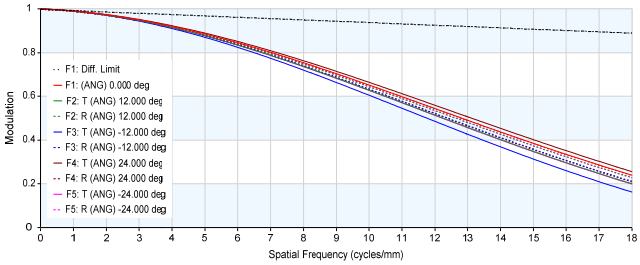

(b)

Figure 4. (a) MTF of the real image and (b) MTF of the virtual image.

The distortion, defined as the displacement of image height or ray location, is less than 0.3% in real image and less than 3.0% in virtual image, respectively, according to Fig. 5.

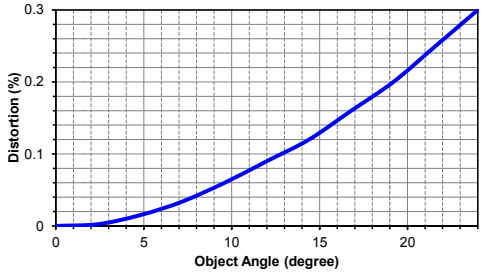

(a)

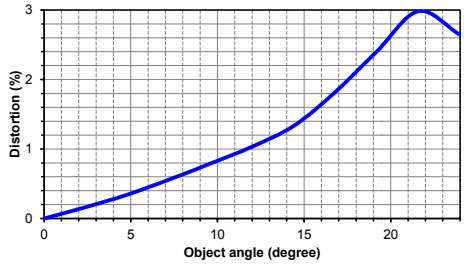

(b)

Figure 5. (a) Distortion of the real image and (b) distortion of the virtual image.

To view the imaging quality, the imaging simulation is performed, as shown in Fig. 6. By comparing the original and simulated images, it can be seen that the real image is almost identical to the original one, while the virtual image becomes blurred and distorted. A feasible technique to mitigate the distortion is to pre-distort the original image.

(a)

(b)

(c)

Figure 6. (a) Original image, (b) real image, and (c) virtual image.

5. Conclusions

A compact design of see-through NED, featuring a curved, reflective surface as an in-coupler and multiplexed VHs as an out-coupler, has been proposed. Based on the simulations, its key performance including DE, FOV, MTF, and distortion has been studied. For real image, MTF is above 0.4 at 140 cycles/mm, and distortion is less than 3.0%. For virtual image, FOV is 54° (diagonal), MTF is above 0.4 at 13 cycles/mm, and distortion is less than 0.3%. By eliminating the need for extra glasses or contact lens, this type of see-through NED could be particularly appealing to the users who suffers from the myopia. Whereas a monocular structure is exemplified in this paper, binocular solution can be realized as well by adding another waveguide to the left of the current one.

6. Acknowledgements

This work is sponsored by Ministry of Science and Technology of the People's Republic of China (MOST) (2013CB328804, 2015AA017001); Shanghai Rockers Inc. (15H100000157).

7. References

[1] K. Kiyokawa, Y. Kurata, and H. Ohno, "An optical see-through display for mutual occlusion with a real-time stereovision system," Comput. Graph. **25**(5), 765–779 (2001).

[2] S. Liu, H. Hua, and D. Cheng, "A novel prototype for an optical see-through head-mounted display with addressable focus cues," IEEE Trans. Vis. Comput. Graph. **16**(3), 381–393 (2010).

[3] H.-S. Chen, Y.-J. Wang, P.-J. Chen, and Y.-H. Lin, "Electrically adjustable location of a projected image in augmented reality via a liquid-crystal lens," Opt. Express **23**(22), 28154–28162 (2015).

[4] Y. Amitai, S. Reinhorn, and A. A. Friesem, "Visor-display design based on planar holographic optics," Appl. Opt. **34**(8), 1352–1356 (1995).

[5] Y. Amitai, "Extremely compact high-performance HMDs based on substrate-guided optical element," SID Symposium (2004), pp. 310–313.

[6] H. Mukawa, K. Akutsu, I. Matsumura, S. Nakano, T. Yoshida, M. Kuwahara, and K. Aiki, "A full-color eyewear display using planar waveguides with reflection volume holograms," J. Soc. Inf. Disp. **17**(3), 185–193 (2009).

[7] D. Cheng, Y. Wang, C. Xu, W. Song, and G. Jin, "Design of an ultra-thin near-eye display with geometrical waveguide and freeform optics," Opt. Express **22**(17), 20705–20719 (2014).

[8] N. Zhang, J. Liu, J. Han, X. Li, F. Yang, X. Wang, B. Hu, and Y. Wang, "Improved holographic waveguide display system," Appl. Opt. **54**(12), 3645–3649 (2015).

[9] A. Maimone, D. Lanman, K. Rathinavel, K. Keller, D. Luebke, and H. Fuchs, "Pinlight displays: wide field of view augmented reality eyeglasses using defocused point light sources," ACM Trans. Graph. **33**(4), 89 (2014).

[10] M. Sugawara, M. Suzuki, and N. Miyauchi, "Retinal imaging laser eyewear with focus-free and augmented reality," SID Display Week (2016), pp. 164–167.

[11] C. P. Chen, Y. Li, Y. Su, G. He, J. Lu, and L. Qian, "Transmissive Interferometric Display with Single-Layer Fabry-Pérot Filter," J. Disp. Technol. **11**(9), 715–719 (2015).

[12] C. Chen, H. Li, Y. Zhang, C. Moon, W. Y. Kim, and C. G. Jhun, "Thin-film encapsulation for top-emitting organic light-emitting diode with inverted structure," Chin. Opt. Lett. **12**(2), 022301 (2014).

[13] C. P. Chen, Z. Zhang, and X. Yang, "A head-mounted smart display device for augmented reality," CN Patent 201610075988.7 (2016).

[14] L. Zhou, C. P. Chen, Y. Wu, K. Wang, and Z. Zhang, "See-through near-eye displays for visual impairment," The 23rd International Display Workshops in conjunction with Asia Display (2016), pp. 1114–1115.

[15] L. Zhou, C. P. Chen, Y. Wu, Z. Zhang, K. Wang, B. Yu, and Y. Li, "See-through near-eye displays enabling vision correction," Opt. Express **25**(3), 2130–2142 (2017).

[16] J. W. Goodman, Introduction to Fourier Optics 3rd Edition (Roberts & Company Publishers, 2004).

[17] W. Hu, C. P. Chen, Y. Li, Z. He, X. Li, P. Zhou, J. Lu, and Y. Su, "Improvement of diffraction efficiency of flat-panel coherent backlight for holographic displays," Opt. Express **23**(4), 4726–4735 (2015).

[18] L. Li, "New formulation of the Fourier modal method for crossed surface-relief gratings," J. Opt. Soc. Am. A **14**(10), 2758–2767 (1997).